International Journal of Thermophysics, Vol. 22, No. 3, 2001

Physical Properties of Basalt and Numerical Simulation of the Melting Process in Basalt Particle Beds

Q. Y. Yan,[1, 2, 3] H. P. Tan,[1] and D. K. Shang[4]

Received April 19, 2000

The physical properties of basalt, such as density, viscosity, permeability, and heat conductivity, were studied experimentally. By introducing the measured parameters into the governing equations of the finite differential method (FDM), the melting processes of basalt, in relation to the thermal boundary conditions and particle sizes, were simulated for the purpose of designing a melting furnace for basalt. The governing equations were discretized in a tridiagonal matrix form and were solved using the tridiagonal matrix algorithm (TDMA) and the alternative direction implicit (ADI) solver. The temperature distribution, position of the two-dimensional phase-change boundary, and melting time were calculated during the numerical simulation. These provide the basis for determining the heating procedure, for controlling the furnace temperature, and for predicting basalt melting states. In the experiment, an electrical furnace was designed based on the computations. It is demonstrated that the simulation results are reasonably consistent with the observed data.

KEY WORDS: basalt; basalt particle bed; melting process, numerical simulation; physical properties.

[1] College of Energy Science and Engineering, Harbin Institute of Technology, 92 West Dazhi Street, Nangang Dist., Harbin 150001, People's Republic of China.

[2] Department of Urban Construction Engineering, Beijing Institute of Civil Engineering and Architecture, No. 1 Zhanlanguan Road, Xicheng District, Beijing 100044, People's Republic of China.

[3] To whom correspondence should be addressed. E-mail: uced@mail.bicea.net.cn

[4] Department of Thermal Engineering, Hebei University of Technology, 1 Ding Zi Gu Road, Tianjin 300130, People's Republic of China.

0195-928X/01/0500-0995$19.50/0

1. INTRODUCTION

Basalt is a natural rock with a variable composition, containing 55% SiO_2, 13% Al_2O_3, etc. It can be processed into fiber through wire-drawing after melting. Wire-drawn basalt fiber can be used in various applications because of its superior properties, i.e., incombustibility, corrosion resistance, high strength, and good thermal and sound insulation [1]. At present, however, research on the production of basalt fiber is rather limited. The melting process of basalt rock influences the stability of fiber drawing as well as the quality of the final fiber products. Therefore, further studies on it are needed.

Many researchers have studied the melting processes of metal and glass with regard to different boundary conditions by numerical simulations or experiments [2–6]. However, studies on the melting of basalt at high temperatures are not available. The melting process of basalt involves heat conduction, heat convection, heat radiation, phase change, dynamic moving boundaries, and interactions among these factors.

Basalt is a noncrystalline solid. Therefore, it has a glassy melting behavior. Over the range of its glassiness, the phases of solid and liquid basalt may unsteadily coexist in a crucible. Since the basalt bed is composed of particles and forms a porous medium, the influence of natural convection needs to be considered in the solid phase. The density of basalt liquid is higher than that of basalt particles, and therefore, during melting, the level of the basalt in the crucible will decrease. Consequently, the calculation domain changes continually. Moreover, the thermophysical parameters are functions of temperature.

In light of the complexities of the problem, the mathematical equations which govern melting processes were defined and then solved numerically. Studies on the physical properties of basalt material from China were not found. These parameters are important in studying the heat transfer process in basalt particle beds.

2. EXPERIMENTAL RESEARCH ON THE PHYSICAL PROPERTIES OF BASALT

2.1. Density and Melting Temperature of Basalt

Density can be defined as

$$\rho = \frac{m}{V} \tag{1}$$

where

$$\rho = \text{density of material } (\text{kg} \cdot \text{m}^{-3})$$

$$m = \text{mass of material } (\text{kg})$$

$$V = \text{volume of material } (\text{m}^3)$$

When the weight m and the volume V of basalt are measured, the density of material can be determined by Eq. (1). Experimental results showed that the density of liquid basalt is higher than that of solid basalt. The density of liquid basalt is 2760.4 $\text{kg} \cdot \text{m}^{-3}$ at 1300°C, and the density of solid basalt is 2704.7 $\text{kg} \cdot \text{m}^{-3}$ at room temperature.

The density of a basalt particle bed that is composed of basalt particles and air is defined as

$$\rho_s = \rho_{air}\sigma_v + (1 - \sigma_v)\,\rho_b \tag{2}$$

where ρ_s, ρ_{air}, and ρ_b are the densities of the basalt particle bed, air, and solid basalt, respectively; σ_v is the porosity. After the porosities of basalt particle beds with different particle sizes are measured by the method of penetration, the densities of particle beds can be determined. When the means of the size distribution of basalt particles d_p are 2.5 and 7.5 mm, the porosities are 42 and 47%, and the densities are 1566 and 1431 $\text{kg} \cdot \text{m}^{-3}$, respectively. It is assumed that the density of liquid, solid, and particle beds of basalt are constants at different temperatures.

Melting of basalt occurs over a wide range of temperature, and in this range, solid and liquid phases can coexist. The melting temperature was measured using an electrical furnace, a crucible, a thermocouple, and a temperature controller. Experimental results show that the melting temperature of basalt is from 1000 to 1260°C.

2.2. Viscosity of Basalt

The viscosity and the variation of the viscosity with temperature and chemical composition are of great importance in the application and production of basalt products. Viscosity can be evaluated through calculation or experiment. Some methods of calculating viscosity according to composition have been developed successfully. However, the methods are normally confined to dealing with a limited number of components over a limited range of viscosity [7–11]. On the other hand, the accuracy of the calculation method is another factor that should be considered. As such, experimental methods are usually used to determine accurate viscosities.

Table I. Chemical Compositions of Samples (wt%)

Sample	SiO_2	Al_2O_3	FeO	Fe_2O_3	CaO	Na_2O	K_2O	MgO	TiO_2	Others
No. 1	45.5	15.2	8.75	8.35	9.4	2.75	1.4	7.8	—	0.85
No. 2	47.99	15.65	8.51	8.53	8.515	1.584	0.63	7.05	0.41	1.11
No. 3	44.0	15.7	8.54	8.41	12.47	1.58	0.68	7.98	—	0.64

In our experiment, the rotational viscometer was used to measure the viscosity of basalt melt. Samples with different compositions were tested: No. 1, basalt; No. 2, basalt + 10% brick; and No. 3, basalt + 10% blast furnace slag. Their chemical compositions are given in Table I.

Experimental results are shown in Figs. 1 and 2. Figure 1 indicates that the viscosity of basalt melt decreases with increasing temperature. When 10% brick is added to the basalt, the quantity of SiO_2 (up to 47.99%) increases, and the viscosity increases. When 10% blast furnace slag is added to basalt, the quantity of CaO (up to 12.47%) increases, and the viscosity decreases. A slight variation in the composition of basalt gives rise to sharp variations in its viscosity.

Figure 2 shows the relationships between viscosity and temperature of three samples on a log–log plot. In the figure, the experimental results show good linear functions. The linear relationships of these three samples can be regressed as follows.

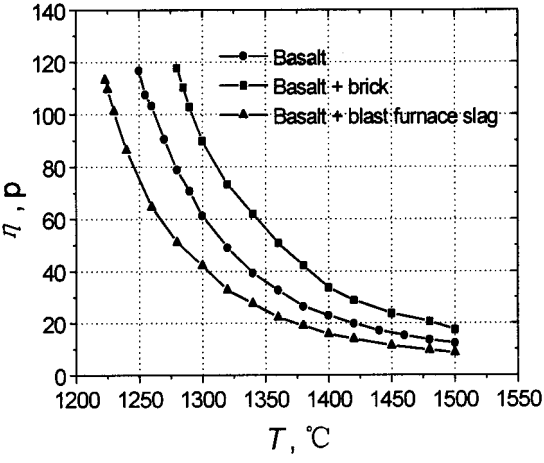

Fig. 1. Relationships between viscosities and temperatures of the three samples.

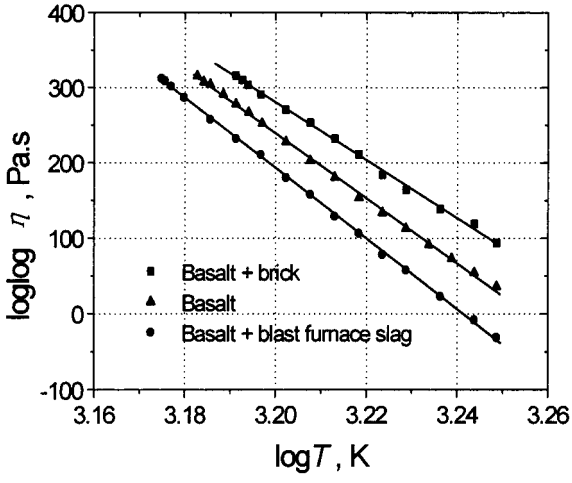

Fig. 2. Relationships between viscosities and temperatures on a log–log plot.

$$\text{Basalt:} \quad \log\log\eta = 14.03 - 4.31\log T \tag{3}$$

$$\text{Basalt + brick:} \quad \log\log\eta = 12.60 - 3.85\log T \tag{4}$$

$$\text{Basalt + blast furnace slag:} \quad \log\log\eta = 15.14 - 4.67\log T \tag{5}$$

where T is the temperature (K) and η is the viscosity (Pa · s; 1 Pa · s = 10 P). Thus, we can use the linear function to predict the viscosity at temperatures outside of the measured range. The equations can be used over a range of viscosity of 10^2 to 10^8 P [12].

2.3. Permeability of Basalt Beds

The permeability of basalt beds is one of the key characteristic parameters for the study of heat transfer processes in basalt beds. In this paper, the experimental equipment developed in our laboratory was used to measure the permeabilities of basalt beds with different particle sizes [13]. The equipment is shown in Fig. 3.

According to Darcy's law, the permeability of a basalt bed is defined as

$$K = \frac{J\mu L}{(\Delta P_b - \Delta P_e)} \tag{6}$$

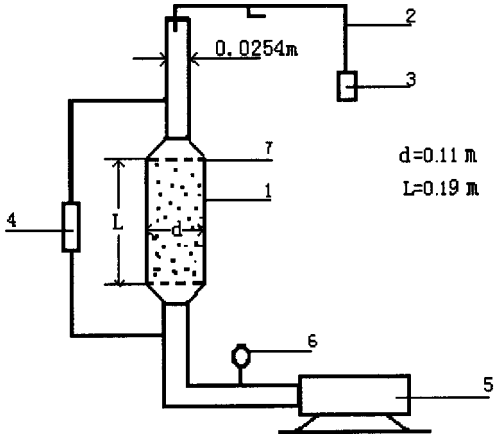

Fig. 3. Experimental equipment. (1) Particle bed; (2) BT tube; (3) slit pressure meter; (4) U-tube pressure meter; (5) air compressor; (6) pressure gauge; (7) metal net.

where

$$K = \text{permeability of the particle bed } (\mathrm{m}^2)$$

$$J = \text{volumetric airflow rate } (\mathrm{m}^3 \cdot \mathrm{m}^{-2} \cdot \mathrm{s}^{-1})$$

$$\Delta P_b, \Delta P_e = \text{pressure differences between the inlet and the outlet of a filled and an empty particle bed, respectively } (\mathrm{Pa})$$

$$\mu = \text{dynamic viscosity of flowing fluid } (\mathrm{Pa} \cdot \mathrm{s})$$

$$L = \text{characteristic length of the particle bed } (\mathrm{m})$$

When ΔP_b, ΔP_e, and J are measured, the permeability K can be determined. The experimental results for different particle sizes are shown in Figs. 4 and 5 and Table II. The relationship between the volumetric airflow rate and the pressure gradient is illustrated in Fig. 4. The figure shows that if the volumetric airflow rate is lower, the pressure gradient and the volumetric airflow rate have an approximately linear relationship. Thus, the flow of fluid in porous media can be described by Darcy's law, and the method of determining the permeability in the paper is reliable. The relationship between the volumetric airflow rate and the permeability is shown in Fig. 5. The figure reveals that when the volumetric airflow rate increases, the permeability will decrease.

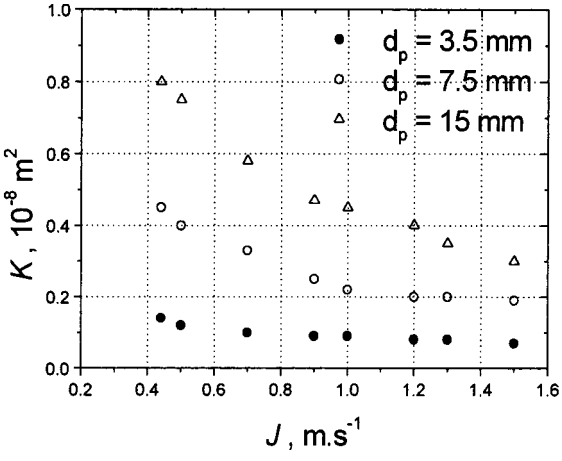

Fig. 4. Relationship between the volumetric airflow rate and the pressure gradient.

The influence of the particle size distribution, density, and porosity on the permeability of basalt particle bed is given in Table III, which illustrates that the permeability increases as the particle size and porosity increase. Porosity is related to particle size and density. With an increase in the particle size, the density decreases while the porosity increases.

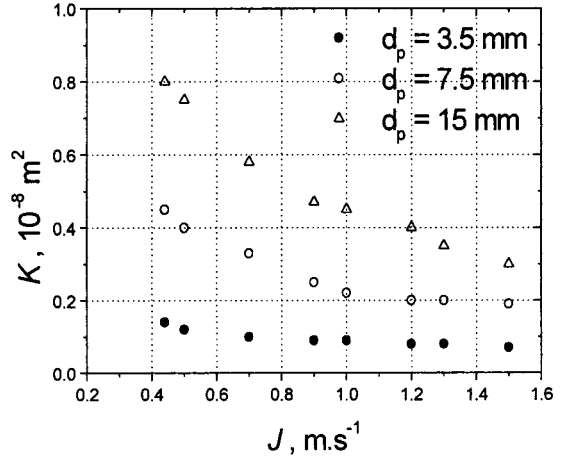

Fig. 5. Relationship between the permeability and the volumetric airflow rate.

Table II. Dependence of Permeability on Particle Size

Particle size (mm)	Density ($kg \cdot m^{-3}$)	Porosity (%)	Permeability ($10^{-9}\ m^2$)
3.5	1469	45.56	0.7
7.5	1457	46.04	1.9
15	1377	49.01	3.03
7.5 (50%) and 15 (50%)	1454	46.15	1.06

2.4. Effective Heat Conductivity of Basalt Beds

According to the Fourier law, the effective heat conductivity of a basalt particle bed can be defined by the following equation:

$$k_s = \frac{Q\delta}{F(T_1 - T_2)} \tag{7}$$

where

Q = heat transferred by conduction (W)

δ = thickness of the medium (m)

F = surface area of the medium (m^2)

T_1 = temperature in the high-temperature end of the medium (°C)

T_2 = temperature in the low-temperature end of the medium (°C)

In the measurement, heat transferred by conduction was determined by measuring the heat absorbed by a heat exchanger. The temperature of the cooling water, which passes through the heat exchanger, increases on absorbing the heat. The heat absorbed by the heat exchanger is

$$Q = \rho_w W c_{pw} \Delta T \tag{8}$$

Table III. Parameters Used in the Calculation of the Permeability of Basalt Beds

k_s ($W \cdot m^{-1} \cdot K^{-1}$)	ρc_p ($J \cdot m^{-3} \cdot K$)	L (m)	β (K^{-1})	M ($m^2 \cdot s^{-1}$)	ΔT (K)
0.8	1.12×10^{-3}	0.16	7.32×10^{-4}	18.1×10^{-6}	715

where

ρ_w = density of water ($kg \cdot m^{-3}$)

c_{pw} = specific heat of water ($J \cdot kg^{-1} \cdot K^{-1}$)

W = volumetric flow of water ($m^3 \cdot s^{-1}$)

ΔT = temperature increase in water after absorbing the heat (°C)

Combining Eqs. (7) and (8), we have

$$k_s = \frac{\rho_w W c_{pw} \Delta T \delta}{F(T_1 - T_2)} \tag{9}$$

In Eq. (9), the density and the specific heat of water and the thickness and surface area of the sample medium are known. The temperature difference between the two ends of the sample, the water flow, and the increase in the temperature of the flowing water in the heat exchanger are measured to determine the effective heat conductivity of the medium using Eq. (9).

Two samples of basalt particles, with $d_p = 2.5$ mm and $d_p = 7.5$ mm, were measured. The experimental results for these two basalt beds are shown in Fig. 6. The effective heat conductivities of basalt particle beds show a linear variation with respect to temperature. After the temperature increases to above 100°C, the values are lower when the particle sizes are

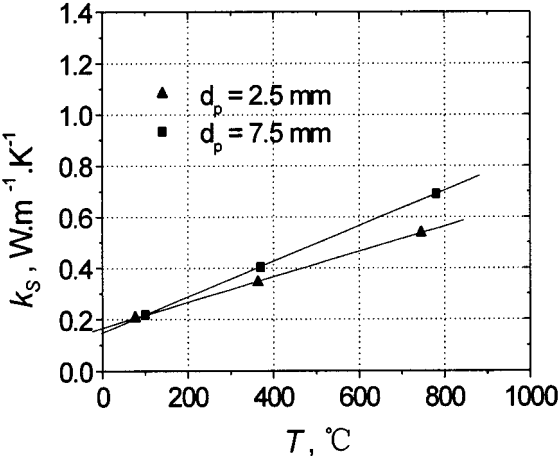

Fig. 6. Effective heat conductivity of basalt beds.

smaller. The experimental results shown in Fig. 6 for these two samples can be regressed as follows:

$$d_p = 2.5 \text{ mm:} \qquad k_s = 0.17 + 4.96 \times 10^{-4} T \tag{10}$$

$$d_p = 7.5 \text{ mm:} \qquad k_s = 0.15 + 6.84 \times 10^{-4} T \tag{11}$$

3. MATHEMATICAL MODELS OF BASALT MELTING

3.1. Experimental Furnace and Heating Mechanisms

A schematic of the experimental furnace is shown in Fig. 7. The crucible was heated mainly by radiation from electrodes and by convection of hot air around the crucible. Within the basalt particles in the crucible, heat may be transported by conduction, radiation, and free convection. Because the effect of free convection on heat transfer depends on the permeability of the basalt particle bed, it is evaluated using the criterion number Ra^H. The criterion number, which is the ratio of heat transferred by free convection to that transferred by conduction, is defined as [14]

$$Ra^H = \left(\frac{\rho_{air} c_{pair}}{k_s}\right)\left(\frac{K \rho_{air} g}{\mu \beta \Delta T}\right) L \tag{12}$$

where

K = permeability of the porous medium (m^2)

k_s = effective heat conductivity of the basalt particle bed ($W \cdot m^{-1} \cdot K^{-1}$)

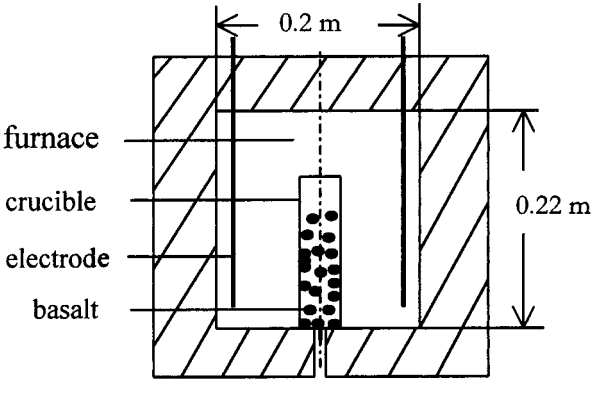

Fig. 7. Schematic of the furnace.

L = height of the basalt particle bed (m)

ΔT = temperature difference along the basalt particle bed (K)

β = volume expansion coefficient (K^{-1})

μ = dynamic viscosity of air ($m^2 \cdot s^{-1}$)

ρc_p = heat capacity of air ($J \cdot m^{-3} \cdot K^{-1}$)

If $Ra^H \ll 1$, then

$$K \ll \frac{k_s/\rho_{air} c_{pair}}{L} \left(\frac{\mu}{\rho_{air} g} \right) \beta \Delta T \tag{13}$$

The natural convection should have a limited effect on heat transport in porous media. By introducing the relevant parameters (Table IV), and if the permeability of the basalt particle bed follows the relation, $K \ll 4.1 \times 10^{-8}\ m^2$, then the natural convection can be neglected.

According to the experimental results, when the mean of the size distribution of basalt particles is less than 7.5 mm, the permeabilities of basalt beds are about $10^{-9}\ m^2$ and decrease with decreasing basalt particle sizes. Therefore, it is reasonable to neglect the natural convection in this work.

3.2. Simplifications and Assumptions

(1) It was assumed that the temperature variations along the r and x coordinates were variable.

(2) It was assumed that the bottom of the crucible was adiabatic because of good insulation.

(3) Because the change in temperature was small in the liquid phase of basalt, it was assumed that the density of liquid basalt was constant.

Table IV. Parameters Used in the Calculations

d_p (mm)	k_s ($W \cdot m^{-1} \cdot K^{-1}$)	ρ_s ($kg \cdot m^{-3}$)	c_s ($kJ \cdot kg^{-1} \cdot K^{-1}$)	Λ ($kJ \cdot kg^{-1}$)	k_l ($W \cdot m^{-1} \cdot K^{-1}$)	ρ_l ($kg \cdot m^{-3}$)	c_l ($kJ \cdot kg^{-1}\ K^{-1}$)
2.5	$0.17 + 4.96 \times 10^{-4} T$	1566	$0.85 + 7.5 \times 10^{-4} T$	531.8	2.0	2760	1.8
7.5	$0.15 + 6.84 \times 10^{-4} T$	1431					

(4) As discussed above, the effect of natural convection in the solid basalt particle bed was neglected due to the low air permeability.

(5) The effect of natural convection in the liquid basalt phase on heat transfer in the crucible was neglected.

3.3. Governing Equations

Basalt is a glassy solid; its phase change occurs over a wide range of temperatures. The melting of basalt occurs between 1000 and 1260°C. The heat capacity method [15] was used to solve the problem. When a unified equation was defined over the entire computation domain, a nonlinear single-phase problem was thus formulated. The phase-change boundary was then determined after determining the temperature distribution. The gevering equation which describes the process is

$$C^* \frac{\partial T}{\partial \tau} = \frac{1}{r} \frac{\partial}{\partial r} \left(k^* r \frac{\partial T}{\partial r} \right) + \frac{\partial}{\partial x} \left(k^* \frac{\partial T}{\partial x} \right) \tag{14}$$

The initial condition is

$$\tau = 0, \qquad T = T_0 \tag{15}$$

and the boundary conditions are

$$r = 0, \qquad \frac{\partial T}{\partial r} = 0 \tag{16}$$

$$r = \mathrm{R}, \qquad k^* \frac{\partial T}{\partial r} = \alpha_{\mathrm{R}}(T)(T_{\mathrm{f}} - T) \tag{17}$$

$$x = 0, \qquad \frac{\partial T}{\partial x} = 0 \tag{18}$$

$$x = \mathrm{l}, \qquad k^* \frac{\partial T}{\partial x} = \alpha_{\mathrm{l}}(T)(T_{\mathrm{f}} - T) \tag{19}$$

where

C^* = equivalent heat capacity ($\mathrm{J \cdot m^{-3} \cdot K^{-1}}$)

k^* = equivalent effective thermal conductivity ($\mathrm{W \cdot m^{-1} \cdot K^{-1}}$)

t_{f} = heating temperature of air around the crucible (K)

α_{l} = coefficient of heat transfer in the top of the crucible ($\mathrm{W \cdot m^{-2} \cdot K^{-1}}$)

α_{R} = coefficient of heat transfer in the circumference ($\mathrm{W \cdot m^{-2} \cdot K^{-1}}$)

3.4. Determination of Thermophysical Parameters

3.4.1. Equivalent Heat Capacity

When the range of melting temperature is from T_m to $T_m + \Delta T$, the equivalent heat capacity can be defined as

$$C^* = \begin{cases} C_s(T), & T < T_m \\ \dfrac{\rho_1 \lambda}{\Delta T} + C_l(T_m), & T_m < T < T_m + \Delta T \\ C_l(T), & T > T_m + \Delta T \end{cases} \tag{20}$$

When the volume fraction of the air component in the basalt bed, which is the porosity, σ_v, is known, the volume of basalt solid in the bed will be $(1\text{-}\sigma_v)$. Then the specific heat of the basalt particle bed is given by [16]

$$\rho_s c_s = \rho_{air} c_{air} \sigma_v + (1 - \sigma_v) \rho_b c_b \tag{21}$$

where

$$c = \text{specific heat } (\text{J} \cdot \text{kg}^{-1} \cdot \text{K}^{-1})$$
$$C = \text{heat capacity } (\text{J} \cdot \text{m}^{-3} \cdot \text{K}^{-1})$$
$$\lambda = \text{latent heat } (\text{J} \cdot \text{kg}^{-1})$$

In the equations above, the subscripts s, air, b, and l represent the basalt particle bed, air, solid basalt, and liquid basalt, respectively. The variation of the specific heat of basalt with temperature is given in Ref. 17. Because the density and the specific heat of air are much lower than those of solid basalt, the equation can be written

$$c_s = c_b \tag{22}$$

3.4.2. Equivalent Effective Thermal Conductivity

$$k^* = \begin{cases} k_s(T), & T < T_m \\ k_s(T) + \dfrac{k_l - k_s}{\Delta T}(T - T_m), & T_m < T < T_m + \Delta T \\ k_l(T), & T > T_m + \Delta T \end{cases} \tag{23}$$

In Eq. (23), the effective heat conductivity of the basalt particle bed, k_s, depends on the temperature. The measured values of the effective heat

conductivities were applied in the simulation. The heat conductivity of the basalt melt, k_1, was taken from Ref. 18.

3.4.3. Coefficient of Heat Transfer

The coefficient of heat transfer varied with boundary temperature and was defined as

$$\alpha(T) = \left[(\alpha_r(T) + \alpha_f(T))^{-1} + \frac{\delta_c}{k_c} \right]^{-1} \tag{24}$$

where

α_f = coefficient of heat transfer of free convection ($W \cdot m^{-2} \cdot K^{-1}$)

α_r = coefficient of heat transfer of radiation ($W \cdot m^{-2} \cdot K^{-1}$)

δ_c = wall thickness of the crucible (m)

k_c = heat conductivity of the crucible ($W \cdot m^{-1} \cdot K^{-1}$)

The parameters used in the above equations are given in Table IV.

3.5. Solution of Governing Equation

The calculation domain was divided into a number of control volumes. The grid spacings and control volumes are shown in Fig. 8. The space steps are $\Delta x = 0.005$ m and $\Delta r = 0.0015$ m, and the time step is $\Delta\tau = 30$ s. Because the basalt melts and the porosity decreases, the calculation domain in the x direction decreases. The number of grids is 34×22 before the basalt melts. After melting, the control volume ΔV decreases to $(1 - \sigma_v)\,\Delta V$. As

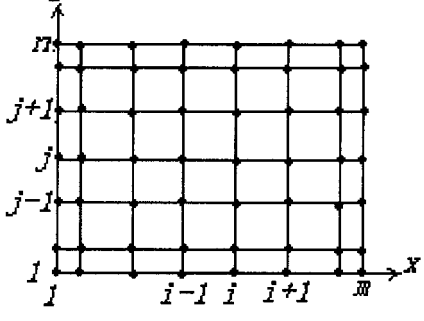

Fig. 8. Grid spacings.

the height of the basalt bed decreases, the number of grid points in the x direction decreases. To keep the space steps Δx and Δr constant, the number of grid points in the x direction was computed again and then the same discretized equations were solved to get the temperature distributions in the new computation domain. The tridiagonal matrix algorithm and the alternative direction implicit solver were used to solve Eqs. (14) to (19).

4. RESULTS AND DISCUSSION

In the numerical simulation, two heating methods are evaluated. In the first one basalt is loaded into the electrical furnace after the furnace temperature increases to the final heating temperature. The computation results are shown in Figs. 9 to 13. In the second method basalt is loaded into the electrical furnace before the electrical furnace is heated. The results are shown in Figs. 14 to 16.

4.1. Temperature Distributions in Basalt Beds in the First Heating Mode

Figure 9 shows the temperature variation with time in the bottom of basalt particle beds with different particle sizes when the heating temperature is 1350°C. After the temperature of basalt in the center rises to above 800°C, the temperatures of basalt particle beds with bigger particle

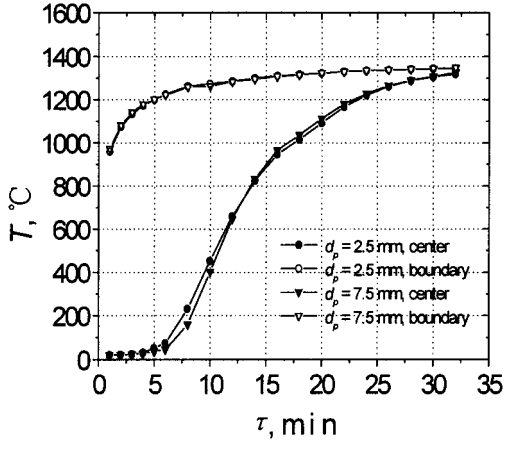

Fig. 9. Temperature distributions of basalt beds with different particle sizes.

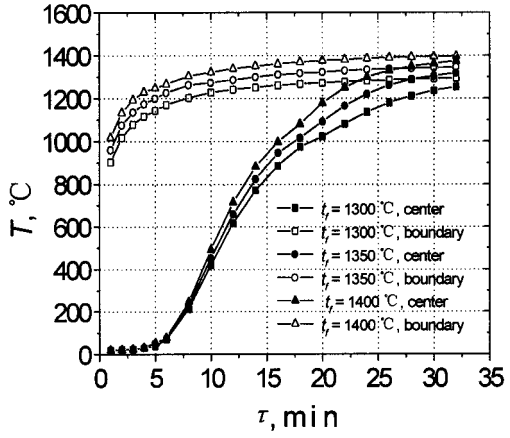

Fig. 10. Temperature distributions for different heating temperatures.

sizes are 10 to 50°C higher than those of beds with smaller particle sizes. However, there are very small temperature differences that are due to different particle sizes. The boundary temperatures of the basalt beds are nearly constant, independent of the particle sizes.

Figure 10 shows the temperature distributions in the bottom of basalt particle beds with $d_p = 2.5$ mm for different heating temperatures. The

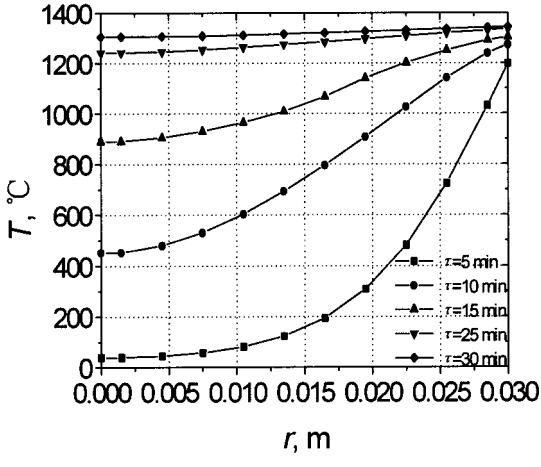

Fig. 11. Temperature distributions in the bottoms of particle beds.

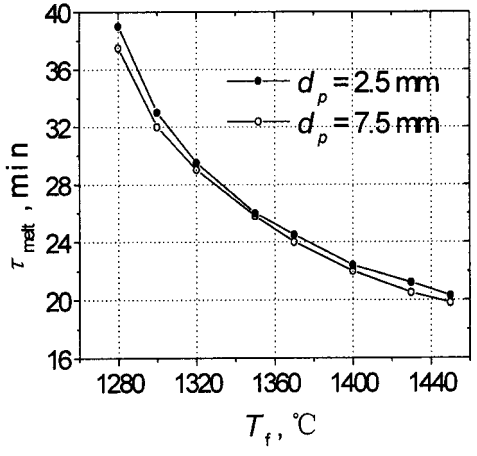

Fig. 12. Melting time for different heating temperatures and particle sizes.

higher the heating temperature is, the higher the material temperatures will be. The temperatures in the boundaries rise rapidly during the first minute, then the temperature remains constant. The temperatures in the center rise slowly; the higher the heating temperature, the faster the temperature increases.

From the above analyses, we know that the effect of particle size and heating temperature on temperature distributions in basalt beds is not significant. Therefore, when basalt melts, raw materials with relatively

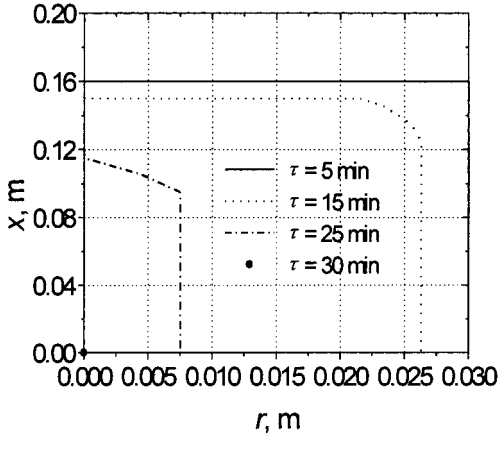

Fig. 13. Dynamic variation of the phase-change boundary.

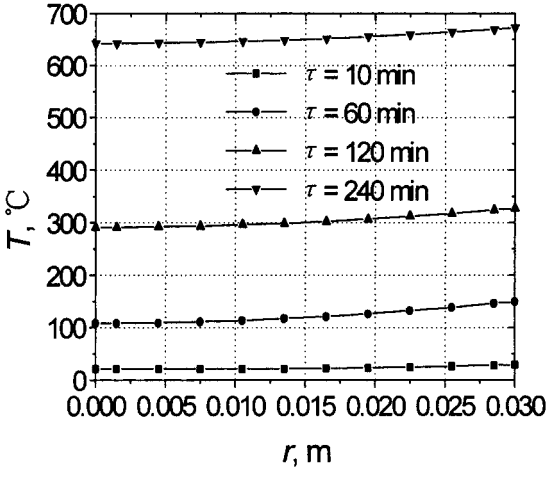

Fig. 14. Temperature distributions in the bottom for the second heating mode.

larger particle sizes may be used. A suitable mean particle size is $d_p = 2.5$ to 7.5 mm. Meanwhile, a very high heating temperature is not necessary. In general, a heating temperature which corresponds to a basalt melt viscosity of about 50 Pa · s is suitable. According to the experimental result, the heating temperature is about 1320 to 1350°C.

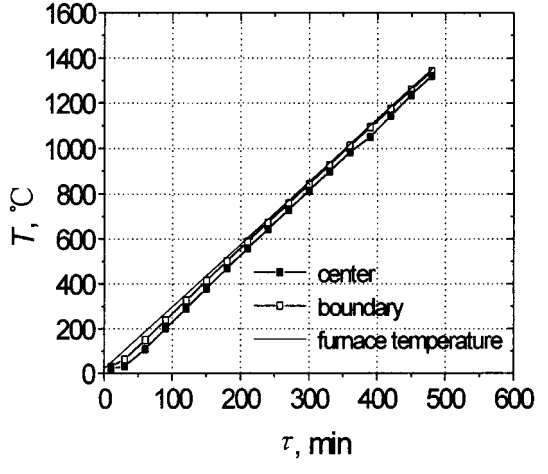

Fig. 15. Temperatures at the center and boundary in the bottom and furnace temperature when the temperature-rise rate is $166°C \cdot h^{-1}$.

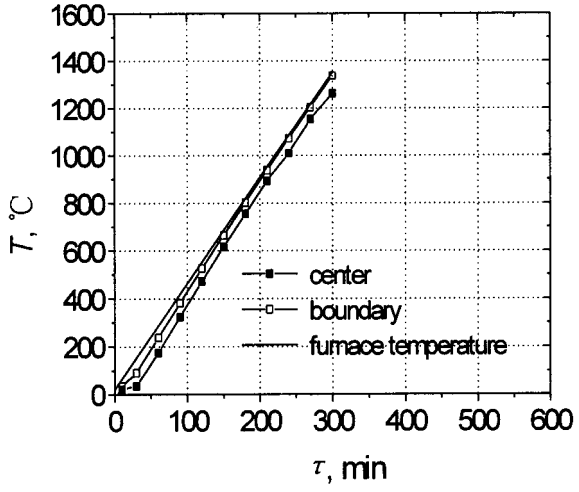

Fig. 16. Temperatures at the center and boundary in the bottom and furnace temperature when the temperature-rise rate is $266°C \cdot h^{-1}$.

Figure 11 shows the temperature distribution along the r direction in the bottom of particle beds where $d_p = 2.5$ mm and the heating temperature is 1350°C. From this figure we see that the temperatures are very uneven in the bottom of the particle bed when heating begins. The temperature difference from the center to the boundary is as high as 1000°C. Although the temperature difference decreases gradually, uneven temperature distributions in the bottoms of beds are maintained for a long time.

4.2. Melting Time and Phase-Change Boundary

Figure 12 shows the relationships among factors such as melting times, particle size distributions, and heating temperatures. From this figure, we see that the higher the heating temperatures are, the shorter the melting time. On the other hand, the melting time decreases with increasing particle sizes, but the difference in melting time with respect to different particle sizes is small for the same heating temperatures.

Figure 13 illustrates the positions of the two-dimensional phase-change boundary when the heating temperature is 1350°C and $d_p =$ 2.5 mm. As the basalt melts, the phase boundary moves to the inner part of the basalt bed along the r and x directions and gets to the center first in the r direction.

4.3. Temperature Distributions in Basalt Beds in the Second Heating Mode

Figure 14 shows temperature variation with time in the bottoms of basalt beds when $d_p = 2.5$ mm and the temperature-rise rate of the electrical furnace is $166°C \cdot h^{-1}$. In the heating process, the temperature distributions along the r direction in the bottoms of basalt beds are constant, and the temperature difference is less than 50°C.

Figures 15 and 16 show the temperatures of the center and boundary in the bottoms of basalt beds and the furnace temperature when the temperature rise rates of the electrical furnace are 166 and $266°C \cdot h^{-1}$, respectively. These figures indicate that the temperature difference is less than 50°C. The more slowly the furnace temperature increases, the smaller the temperature difference.

Based on the above results, we see that the second heating method is more favorable for the production of basalt fiber than the first one. Even temperature distributions within basalt particle beds prevent the base plate from breakage and ensure that the fiber-drawing process is stable. Therefore, the second heating method should be used in experiments.

5. CONCLUSIONS

Based on this study, differences in temperature and melting duration with respect to particle size and heating temperature are not significant. It is suggested that a relatively larger particle size and lower heating temperature can be used for the production process. The use of particles that are too fine may cause entrainment of fine dust during feeding and can increase the handling cost of raw materials. It was observed that a mean particle size $d_p = 2.5$ to 7.5 mm is suitable for the basalt bed. If the heating temperature is too high, the costs of heating electrodes and fireproof materials are high. When the air temperature around the crucible reached 1450°C or even higher, a special refractory composite material of zirconium oxide at a high percentage was used to make the crucible. Heating temperatures of 1320 to 1350°C are suitable. On the other hand, the second heating method is favorable for ensuring a steady fiber-drawing process and preventing breakage of the base plate of the crucible caused by nonuniform temperature distributions.

REFERENCES

1. V. I. Kostikov, *Fiber Science and Technology* (Chapman Hall, London, 1995), pp. 581–583.
2. S. P. Manjhi, N. Ramachandran, R. N. Nalla, M. K. Bajpai, and P. K. Tripathi, *Heat Transfer Eng.* **18**:57 (1997).

3. Y. W. Zhang, Y. Y. Jin, Z. Q. Chen, and Y. B. Yu, *J. Heat Transfer* **115**:463 (1993).
4. X. P. Lin, X. F. Pen, B. X. Wang, and D. Y. Ke, *J. Eng. Thermophys.* **19**:62 (1998).
5. K. O. Lim, T. H. Song, and K. S. Lee, *Glass Tech.* **39**:27 (1998).
6. D. Radu and O. Dumitrescu, *Glass Tech.* **33**:167 (1992).
7. I. V. Mingarro, J. M. Rincon, and P. Bowles, *Glass Tech.* **33**:49 (1992).
8. S. G. Hu and G. R. Chen, *Glass Tech.* **33**:53 (1992).
9. T. Lakatos, L. G. Johansson, and B. Simmingskold, *Glass Tech.* **13**:88 (1972).
10. K. C. Lyon, *J. Res. Natl. Bur. Stand.* **78**:497 (1974).
11. K. C. Lyon, *Ceram. Bull.* **54**:1010 (1975).
12. Y. T. Shi and Z. Y. Yao, *Glass Fiber* **2**:5 (1987).
13. D. K. Shang, Q. Y. Yan, and H. P. Tan, *Holz als Roh-und Werkstoff.* **57**:271 (1999).
14. M. Collin, *Mathematical Modeling of Transport Processes and Degradation Reactions in Piles of Forest Fuel Material* (Stockholm, 1986), pp. 45–47.
15. J. Crank, *Free and Moving Boundary Problems* (Clarendon Press, Oxford, 1984), p. 5.
16. D. K. Shang, Ph.D. thesis (Swedish University of Agricultural Sciences, Garpenberg, 1989), p. 50.
17. T. F. Omar, *Thermal Properties of Soils* (Trans. Tech. Pub., Germany, 1986), p. 87.
18. M. G. Chernek and K. E. Blouhe, Thesis of Science and Research, *BHNNCB* **6**:33 (1959).